# Accurate Modeling of a Transverse Flux Permanent Magnet Generator Using 3D Finite Element Analysis

Seyedmohsen HOSSEINI[1], Javad Shokrollahi MOGHANI[1], Bogi Bech JENSEN[2]
[1]*Electrical Engineering Department, Amirkabir University of Technology, Tehran 15916, Iran*
[2]*Centre for Electric Technology, Technical University of Denmark (DTU), Kongens Lyngby, Denmark*
*m_hosseini@aut.ac.ir*

***Abstract*—This paper presents an accurate modeling method that is applied to a single-sided outer-rotor transverse flux permanent magnet generator. The inductances and the induced electromotive force for a typical generator are calculated using the magnetostatic three-dimensional finite element method. A new method is then proposed that reveals the behavior of the generator under any load. Finally, torque calculations are carried out using three dimensional finite element analyses. It is shown that although in the single-phase generator the cogging torque is very high, this can be improved significantly by combining three single-phase modules into a three-phase generator.**

***Index Terms*—equivalent circuit, finite element method, generators, permanent magnets.**

## I. INTRODUCTION

Transverse flux machines can offer higher power and torque density than conventional radial flux machines [1]-[5]. The torque in a transverse flux machine is nearly proportional to the number of poles [2]. The capability of having large pole numbers, combined with the torque from a transverse flux permanent magnet generator (TFPMG) being almost proportional to the number of poles, makes TFPMGs particularly suitable for gearless wind turbines [6], [7].

The flux path in a TFPMG has a three dimensional (3D) nature. Accurate modeling of a TFPMG therefore requires three-dimensional finite element analysis (3D FEA) [8]. The cogging torque of a single phase TFPMG is typically very high, but this is usually improved significantly by combining three single phase modules into a three phase machine [9]-[11].

In this paper, the equivalent circuit parameters of a designed TFPMG are calculated using 3D FEA. The chosen TFPMG topology was proposed by Gieras in [12]. The calculated parameters are used to evaluate the TFPMG's performance characteristics. A new method is then proposed to evaluate the behavior of the generator under any load. In the proposed method two non-linear equations are solved iteratively. The proposed method is used to investigate the output power, output voltage, efficiency and load angle as functions of a varying *RL* load. These results can be used to optimally utilization of the generator for any given load. Finally, the cogging torque is calculated using 3D FEA. It is shown that the cogging torque is very high in a single phase TFPMG, but that this can be significantly reduced by combining three single phase modules into a three phase machine.

## II. TFPMG CONSTRUCTION

Fig. 1 shows a 3D view of a single-sided outer-rotor TFPMG. Fig. 1, only shows a single phase of the generator.

A three-phase generator can be constructed from three identical single phase modules (Fig. 1) shifted in space by 120 electrical degrees [12], [13]. Nd-Fe-B rare-earth permanent magnets create the generator excitation. Both the stator and the rotor cores are made up from thin steel laminations. The rotor consists of surface mounted permanent magnets (PMs) in two rows. These PMs create homopolar fluxes in stator cores at any time, meaning that the polarity of all the stator cores is identical at any given time. The rotation of the rotor causes a change in the armature winding flux linkage, which induces the armature electromotive force (EMF).

Every phase of the generator has one armature winding which is located between the stator poles and consists of a simple ring-shaped coil. In the TFPMG, the number of PMs in one row is twice the number of stator cores.

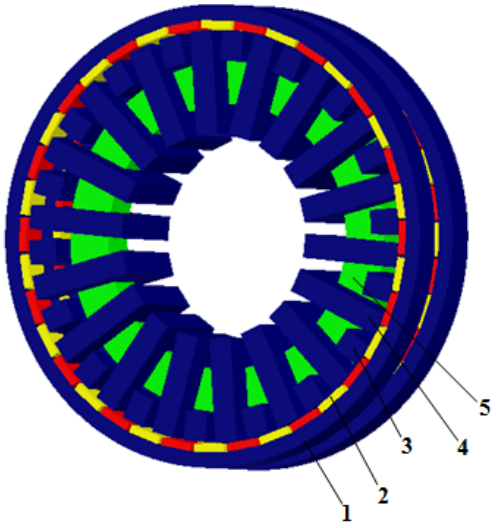


Figure 1. 3D view of a single-sided outer-rotor TFPMG. (1) Rotor core. (2) PM. (3) Stator I-shaped core. (4) Stator U-shaped core. (5) Armature winding.

Let $p$ denote the number of pole pairs (which is equal to half of the number of PMs belonging to one row or the number of stator cores) and $n(rps)$ stands for the rotational speed, then the frequency of output voltage is determined exactly as it would be for a synchronous machine, *i.e.*,

Digital Object Identifier 10.4316/AECE.2011.03019

$$f = n\,p \tag{1}$$

## III. TFPMG MODEL

A per phase equivalent circuit diagram of the TFPMG is shown in Fig. 2. In general $L_{sd}$ and $L_{sq}$ represent the armature winding d- and q-axis inductances, respectively. The d- and q-axis reactances in Fig. 2, $X_{sd}$ and $X_{sq}$, are therefore obtained as below

$$X_{sd} = L_{sd}\,\omega\ ;\ X_{sq} = L_{sq}\omega \tag{2}$$

where $\omega = 2\pi f$ is the angular frequency. In Fig. 2, $I_a$, $R_a$, $V_{out}$, $R_L$, and $X_L$ are the current of the armature winding; the armature winding resistance, the output voltage of the armature winding; the load resistance of the armature winding; and the load reactance of the armature winding, respectively. The induced EMF of the armature winding due to the fundamental flux linkage of PMs in the air-gap is represented by $E_f$. The phasor diagram of one module of the TFPMG loaded with the resistance ($R_L$) and reactance ($X_L$) is shown in Fig. 3.

The associated output voltage projections on the d- and q-axis are

$$\begin{aligned} V_{out}\sin\delta &= I_{aq}\,X_{sq} - R_a\,I_{ad} \\ V_{out}\cos\delta &= E_f - I_{ad}\,X_{sd} - I_{aq}\,R_a \end{aligned} \tag{3}$$

Where $I_{ad}$ and $I_{aq}$ are the projections of the armature current $I_a$ on the d- and q-axis, respectively. The load angle $\delta$ is the angle between the output voltage $V_{out}$ and EMF $E_f$. The output power of one module (phase) is

$$P_{out} = V_{out}\,I_a\cos\phi \tag{4}$$

where $\phi$ is the phase angle between the armature current and the output voltage. In (4), $I_a\cos\phi$ is the projection of $I_a$ on $V_{out}$. Using Fig. 3 this becomes

$$I_a\cos\phi = I_{ad}\sin\delta + I_{aq}\cos\delta \tag{5}$$

Combining (3), (4) and (5) leads to

$$P_{out} = E_f\,I_{aq} - I_{ad}\,I_{aq}\left(X_{sd} - X_{sq}\right) - R_a\,I_a^2 \tag{6}$$

The internal electromagnetic power of one module of the generator, $P_{elm}$, is the sum of the stator winding losses, defined by $\Delta P_{lw} = R_a I_a^2$, the stator core losses, defined by $\Delta P_{lFe}$, and the output power, $P_{out}$.

$$\begin{aligned} P_{elm} &= P_{out} + \Delta P_{lw} + \Delta P_{lFe} = \\ &= E_f\,I_{aq} - I_{ad}\,I_{aq}\left(X_{sd} - X_{sq}\right) + \Delta P_{lFe} \end{aligned} \tag{7}$$

The stator core losses can be calculated if the amplitude and the frequency of the time varying magnetic flux density in the stator core are known. The efficiency is

$$\eta = \frac{P_{out}}{P_{elm} + \Delta P_{rot} + \Delta P_{str}} \tag{8}$$

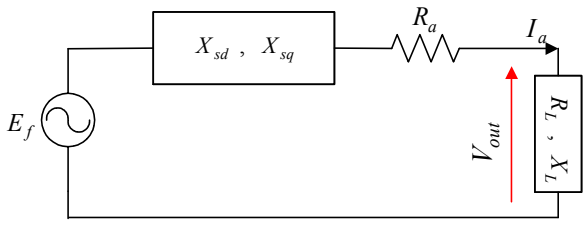


Figure 2. Per phase equivalent circuit diagram of the TFPMG.

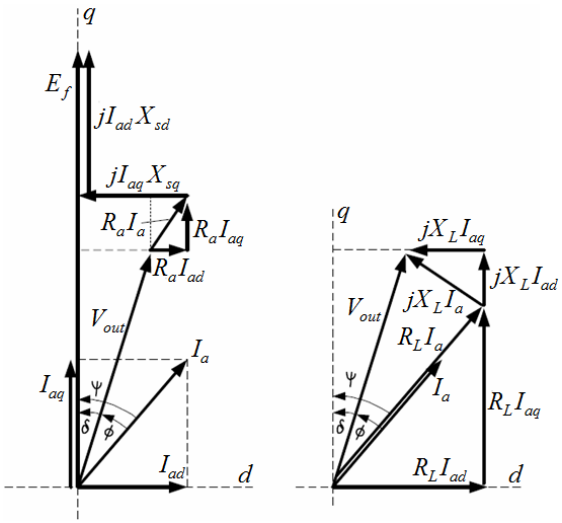


Figure 3. Phasor diagrams of one module of the TFPMG loaded with an RL load.

where $\Delta P_{rot}$ and $\Delta P_{str}$ are rotational losses and stray losses, respectively. The power factor, $PF$, is an important figure of merit of an electrical machine. The value of $PF$ determines the size of control unit and thus the cost of the entire system. The $PF$ is defined as

$$PF = \frac{E_f - R_a\,I_{aq}}{V_{out}} \tag{9}$$

when the armature current is chosen to be in phase with the EMF, *i.e.* armature current is in the q-axis direction only [9].

If in Fig. 3, $V_{out}$ is considered as the reference vector, $I_a$ and its projections on the d- and q-axis as well as $E_f$ become

$$\begin{aligned} \bar{I}_a &= \frac{V_{out}\angle 0^\circ}{R_L + jX_L} = I_a\angle -\phi \\ \bar{I}_{ad} &= I_a\sin(\delta+\phi)\angle\left(-\frac{\pi}{2}+\delta\right) \\ \bar{I}_{aq} &= I_a\cos(\phi+\delta)\angle\delta \\ \bar{E}_f &= E_f\angle\delta \end{aligned} \tag{10}$$

Applying Kirchhoff's voltage law to Fig. 2 yields

$$\begin{aligned} &E_f\angle\delta = \\ &V_{out}\angle 0^\circ + R_aI_a\angle -\phi + jX_{sq}\bar{I}_{aq} + jX_{sd}\bar{I}_{ad} \end{aligned} \tag{11}$$

Combining (10) and (11) while separating into real and imaginary parts gives the two non-linear equations below

$$E_f \sin\delta = -R_a I_a \times \left(\sqrt{1-(\cos(\phi))^2}\right) + X_{sq} I_a \cos\delta \left(\begin{array}{l}(\cos(\phi))\times\cos\delta - \\ \left(\sqrt{1-(\cos(\phi))^2}\right)\sin\delta\end{array}\right) + X_{sd} I_a \sin\delta \left(\begin{array}{l}(\cos(\phi))\times\sin\delta + \\ \left(\sqrt{1-(\cos(\phi))^2}\right)\cos\delta\end{array}\right) \quad (12)$$

,

$$E_f \cos\delta = V_{out} + R_a I_a \times (\cos(\phi)) - X_{sq} I_a \sin\delta \left(\begin{array}{l}(\cos(\phi))\times\cos\delta \\ -\left(\sqrt{1-(\cos(\phi))^2}\right)\sin\delta\end{array}\right) + X_{sd} I_a \cos\delta \left(\begin{array}{l}(\cos(\phi))\times\sin\delta \\ +\left(\sqrt{1-(\cos(\phi))^2}\right)\cos\delta\end{array}\right) \quad (13)$$

The generator behavior under any arbitrary *RL* load (or variation of $I_a$ and $\phi$) can be obtained by first finding the load angle, $\delta$, from (12) and then finding the output voltage from (13). Equation (12) is a non-linear equation and must be solved iteratively [14]. After obtaining $\delta$, the output voltage, $V_{out}$ can be obtained from (13). Knowing $\delta$ and $V_{out}$, it is possible to calculate the generator characteristic performance under any *RL* load.

## IV. Calculation of the Equivalent Circuit Parameters Using 3D Magnetostatic FEA

The geometric dimensions used for this TFPMG are those given in [12].

### A. Inductance Calculation

Synchronous inductances are calculated using the modified incremental energy method [15]. This method consists of the following steps: (1) for a given rotor position $\theta_e$ (rotor electrical angle position), conduct a non-linear field analysis considering the saturation due to the PMs to find the operating point of the machine, and save the incremental permeability in each element; (2) Set the remanence of the PMs to be zero, and conduct a linear field analysis with the saved permeabilities with stator current perturbation, *i.e.* assigning winding current $\Delta i$; (3) Calculate the magnetic co-energy for the current excitation; and (4) Calculate the incremental inductances by:

$$L(\theta_e) = \frac{2W_c(\Delta i, \theta_e)}{(\Delta i)^2} \quad (14)$$

where $\Delta i$ is the nominal current of the armature winding, $\theta_e$ is electrical angle position, and $W_c$ is coenergy. Results of the inductance calculation are given in Table I, where it can be seen that this machine is non-salient.

TABLE I. Results of Inductance Calculation

| | |
|---|---|
| $L_{sd}$ (H) | $77^2 \times 2.9946 \times 10^{-6}$ |
| $L_{sq}$ (H) | $77^2 \times 2.9877 \times 10^{-6}$ |

### B. EMF Calculation

Fig. 4 and Fig.5 illustrate the magnetic flux density in the stator and rotor cores established by the PMs at $\theta_e = 0^\circ$ (maximum excitation) and $\theta_e = 90^\circ$, respectively. In Fig. 6, the no-load flux linkage per turn versus electrical angle is shown. In order to obtain every point of Fig. 6, a 3D magnetostatic FEA is performed.

Fourier analysis of the graph shown in Fig. 6 gives: a fundamental of $\Phi_{f1} = 1.96 \times 10^{-4}\ Wb$ and a total harmonic distortion of $THD = 9.4\%$. $\Phi_{f1}$ is the fundamental harmonic

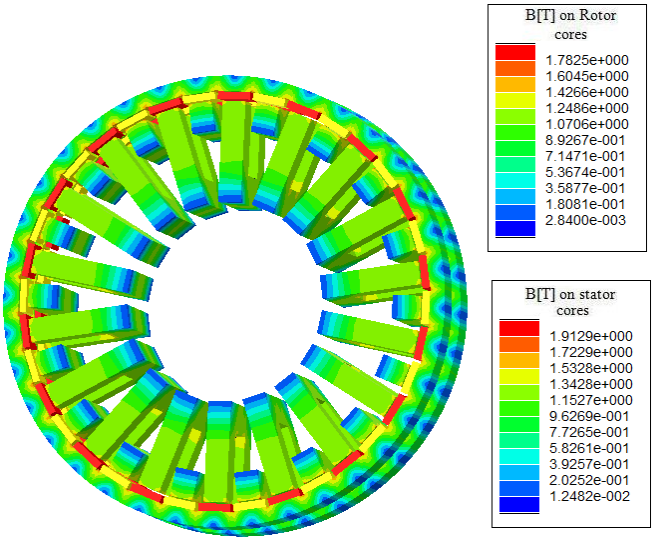


Figure 4. The magnetic flux density in the stator and rotor cores at $\theta_e$=0$^0$.

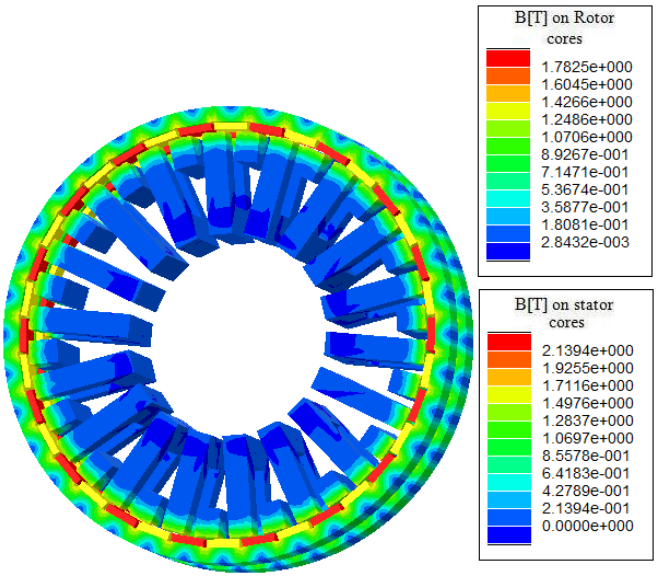


Figure 5. The magnetic flux density in the stator and rotor cores at $\theta_e$=90$^0$.

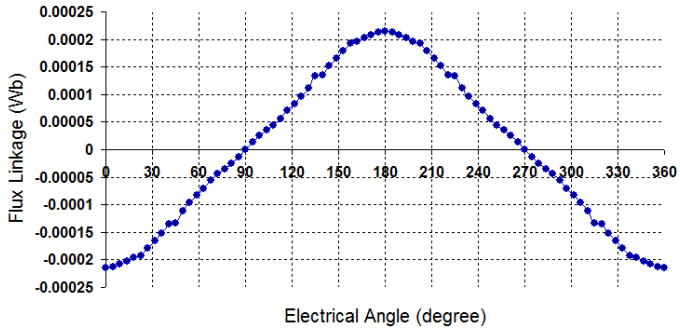


Figure 6. No-load flux linkage per turn versus electrical angle.

of the no-load flux linkage per turn. When the generator is rotated at the speed $\omega_m\left(rad/Sec\right)$, the rms value of the induced EMF of the armature winding is

$$E_f = \frac{p^2 N \omega_m \Phi_{f1}}{\sqrt{2}} \tag{15}$$

where $N$ is the turn number of the armature winding. In the studied TFPMG $p=18$ and $N=77$ [12]. The generator is rotated with the fixed speed 594 rpm. Consequently,

$$E_f = \frac{18^2 \times 77 \times 594 \times \left(\frac{2\pi}{60}\right) \times 1.96 \times 10^{-4}}{\sqrt{2}} = 215\text{V}$$

### C. Core Losses Estimation

The rotation of the rotor causes a varying magnetic flux density in the stator cores (both the U-shaped and the I-shaped cores). Fig. 4 and Fig. 5 demonstrate magnetic flux does not change in rotor cores due to rotor rotation. Therefore core losses only exist in the stator cores. In order to calculate stator core losses, magnetic flux density in stator cores at $\theta_e = 0^\circ$ (maximum excitation) should be calculated. After the 3D magnetostatic FEA (Fig. 4), the magnetic flux density in each node of the meshed area, shown in Fig. 7, is derived. Fig. 8 and Fig. 9 illustrate the magnetic flux density in the U-shaped and the I-shaped stator cores, respectively, for the meshed areas shown in Fig.7. The average value of the maximum flux density, $\overline{B}_m$, is the average of the surface nodes which are shown in Fig. 8 and Fig. 9. Having $\overline{B}_m$ and its variation in frequency determined, it is possible to calculate the core losses using the Steinmetz method. $\overline{B}_m$ in the U-shaped and the I-shaped stator cores as well as the corresponding specific core losses, $\Delta p_{Fe}$, in (W/kg) at the operation frequency, are given in Table II. The operational frequency is $f = n \times p = \left(594/60\right) \times 18 = 178.2\,Hz$.

The stator core losses of one single phase module are

$$\Delta P_{lFe} = \left(\Delta p_{FeU} \times m_U + \Delta p_{FeI} \times m_I\right) \tag{16}$$

where $m_U$, $m_I$, $\Delta p_{FeU}$ and $\Delta p_{FeI}$ are total U-shaped core mass, the total I-shaped core mass, and the specific core losses of U-shaped cores and specific core losses of I-shaped cores, respectively. The calculated total iron losses for this machine were $\Delta P_{lFe} = 84.26\,W$. PMs losses are neglected.

## V. Performance Analysis of the TFPMG

### A. Power Factor and Power Density

In order to compare the power factor of different machines it is common to assume the current is in phase with the EMF ($I_{ad}=0$) the output voltage, $V_{out}$ is

$$V_{out} = \sqrt{\left(E_f - R_a I_{aq}\right)^2 + \left(X_{sq} I_{aq}\right)^2} \tag{17}$$

Power density of a single phase module is the ratio of the module's output power to the module's active material (PMs+ stator and rotor cores+ copper) mass. $R_a$, nominal $I_{aq}$ and mass of active materials are given in [12]. The calculated power factor ($PF$) and power density are given in Table III. These results are in good agreement with experimental results which are given in [12].

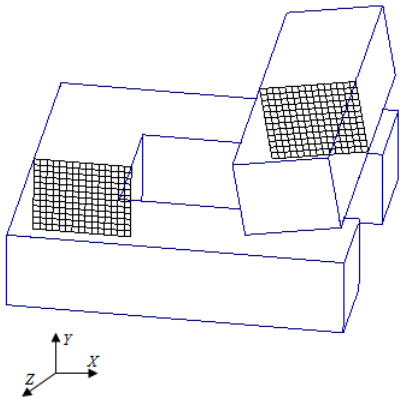


Figure 7. Meshed areas in the U-shaped and I-shaped stator cores.

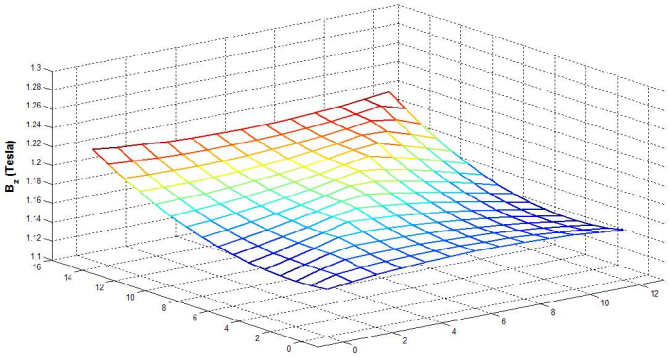


Figure 8. The magnetic flux density in the meshed area of the U-shaped stator core.

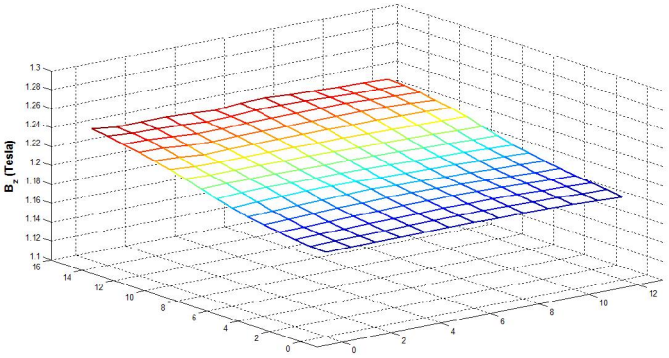


Figure 9. The magnetic flux density in the meshed area of the I-shaped stator core.

TABLE II. SPECIFIC STATOR CORE LOSSES AT THE OPERATION FREQUENCY

| | $\overline{B}_m(T)$ | $\Delta p_{Fe}$ (W/Kg) |
|---|---|---|
| U-shaped Core | 1.176 | 19.351 |
| I-shaped Core | 1.212 | 21.495 |

TABLE III. CALCULATED *POWER FACTOR* AND POWER DENSITY

| | Calculation | Experiment [12] |
|---|---|---|
| *Power Factor* | 0.64 | 0.57 |
| Power Density (kW/Kg) | 0.33 | 0.3 |

### B. *TFPMG Behavior Under RL Load*

Using the described method at the end of section II, the behavior of the TFPMG is investigated for any *RL* load. The rotational losses and the stray losses are estimated to about 66W and 43W, respectively [13]. Fig. 10, Fig. 11, Fig. 12 and Fig. 13 illustrate the variation of load angle, output voltage, per phase output power, and efficiency versus *RL* load current and phase angle, respectively. These figures are very useful for optimal utilization of the TFPMG in different applications. For example, the maximum output power of the TFPMG can be found from Fig. 12 and the maximum efficiency can be found from Fig. 13. The conditions for maximum output power are found using Fig. 12 and displayed in Table IV.

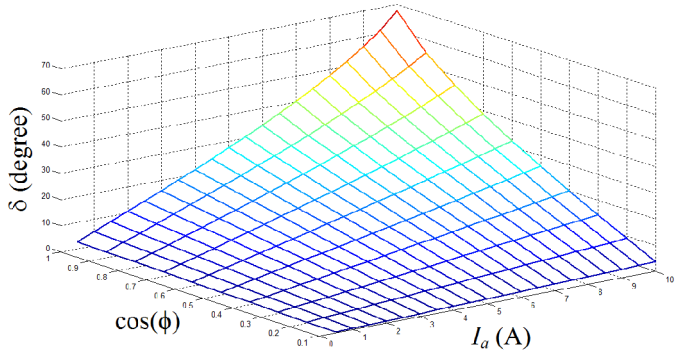


Figure 10. Variation of $\delta$ versus *RL* load current.

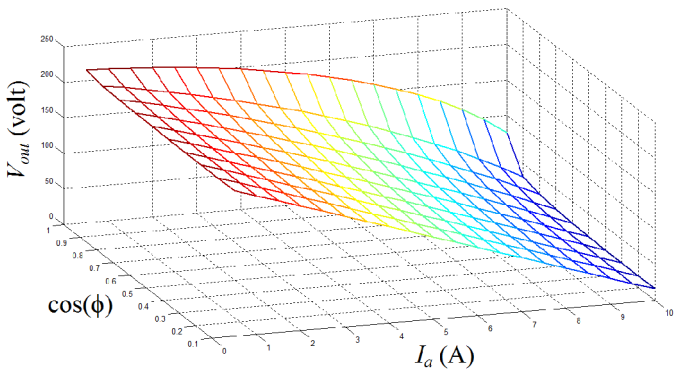


Figure 11. Variation of $V_{out}$ versus *RL* load current.

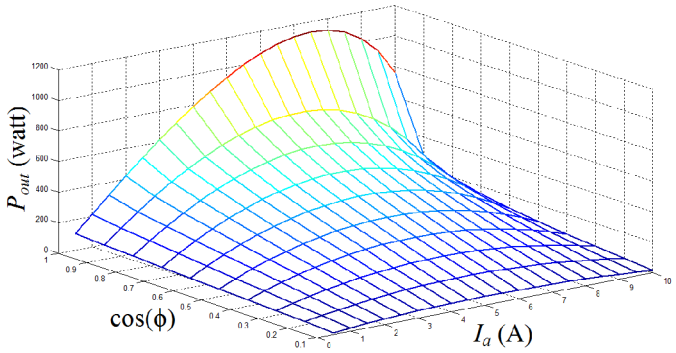


Figure 12. Variation of $P_{out}$ versus *RL* load current.

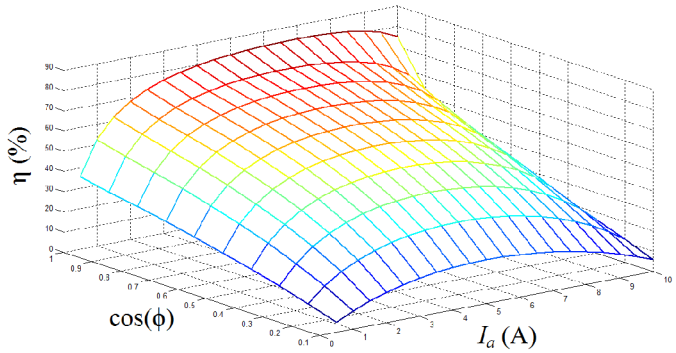


Figure 13. Variation of efficiency versus *RL* load current.

TABLE IV. TFPMG OPERATIONAL INFORMATION FOR DELIVERING MAXIMUM OUTPUT POWER UNDER AN *RL* LOAD

| | |
|---|---|
| $I_a(A)$ | 7.5 |
| $\cos\phi$ | 1 |
| $P_{out}(kW)$ | 1.13 |
| $\eta(\%)$ | 83.24 |
| $\delta(\deg ree)$ | 43.82 |
| $V_{out}(V)$ | 150.48 |

## VI. COGGING TORQUE

The cogging torque of a single phase module versus electrical angle is shown in Fig. 14. The peak cogging torque of one module is very high compared with the average torque of the one module TFPMG (44.8Nm). The cogging torque is so high that the instantaneous torque becomes negative for the electrical angle intervals: $14^\circ < \theta_e < 26^\circ$ and $194^\circ < \theta_e < 206^\circ$. This can be seen in Fig. 14, where the negative cogging torque is shown to be higher than the average torque of 44.8Nm, in the electrical angle intervals: $14^\circ < \theta_e < 26^\circ$ and $194^\circ < \theta_e < 206^\circ$. Constructing a single phase TFPMG of this type would therefore not be wise.

Fig. 15 illustrates the three phase cogging torque variation versus electrical angle. The three-phase cogging torque is obtained by adding three times the cogging torque of a single phase module whilst taking phase shift between them into account [9]. Fig 15 shows that the peak cogging torque of a three phase TFPMG is significantly reduced compared with the single phase module TFPMG. The peak cogging

torque of a single phase module was 121.5% of the average torque (54.45Nm compared to an average of 44.8Nm). A single phase TFPMG of this type would therefore be highly impractical. The peak cogging torque of a three phase machine was 28.6% of the average torque (38.44Nm compared to an average of 134.4Nm). This is still a very high cogging torque, which would result in significant vibrations and noise. Although the cogging torque was not reported in [12], it was still admitted that the cogging torque was too high and resulted in noise and vibrations.

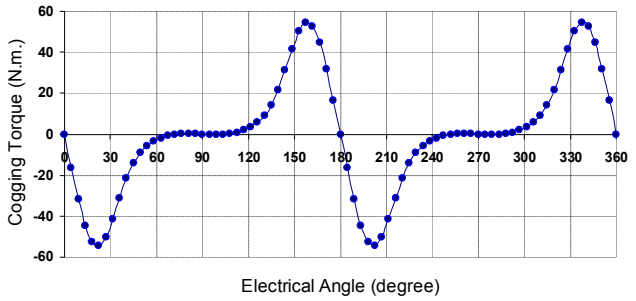


Figure 14. One module cogging torque versus electrial angle

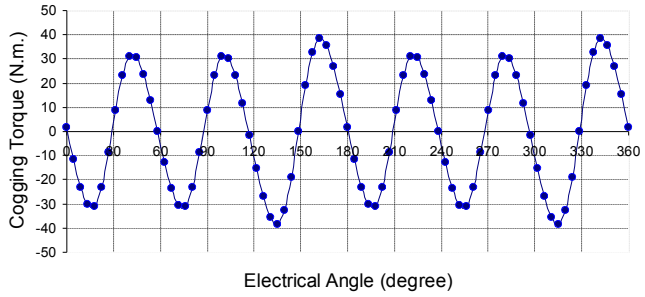


Figure 15. Three phase cogging torque versus elecrical angle

## VII. Conclusion

This paper presents an accurate modeling method applied to a typical TFPMG, with the aid of 3D magnetostatic FEA. Inductances, induced EMF, and the core losses are calculated using 3D FEA. A new method for investigating the behavior of the TFPMG under any *RL* load is presented. The cogging torque analysis shows this type of generator requires a minimum of three phases but would benefit further if a higher number of phases were employed.

## References

[1] I.-A. Viorel, L. Strete, K. Hameyer, "Construction and design of a modular permanent magnet transverse flux generator," Advances in Electrical and Computer Engineering, vol. 10, no. 1, pp. 3-6, 2010. [Online]. Available: http://dx.doi.org/10.4316/AECE.2010.01001

[2] H. Weh, H. Hoffmann, and J. Landrath, "New permanent magnet excited synchronous machine with high efficiency at low speeds, " in Proc. Int. Conf. Electrical Machines, Pisa, Italy, 1990, vol. 3, pp. 35-40.

[3] H. Weh and H. May, "Achievable force densities for permanent magnet excited machines in new configurations," in Proc. Int. Conf. Electrical Machines, ICEM 86, Munich, Germany, 1986, pp. 1107-1111.

[4] W. M. Arshad, T. Backstrom and C. Sadarangani, "Analytical design and analysis procedure for a transverse flux machine," in Proc. IEEE International Conference on Electric Machines and Drives, IEMDC 2001, Cambridge, MA, USA, 2001, pp. 115-121.

[5] S. Hosseini, J. S. Moghani, N. F. Ershad, and B. B. Jensen "Design, prototyping, and analysis of a novel modular permanent-magnet transverse flux disk generator," IEEE Transaction on Magnetics, vol. 47, No. 4, pp. 772-780, May 2011.

[6] D. Svechkarenko, On Analytical Modeling and Design of a Novel Transverse Flux Generator for Offshore Wind Turbines, Licentiate Thesis, Royal Institute of Technology, Stockholm, Sweden, 2007. [Online]. Available: http://kth.diva-portal.org/smash/get/diva2:12332/FULLTEXT01

[7] M. R. Dubois, Optimized Permanent Magnet Generator Topologies for Direct Drive Wind Turbines, Ph.D. dissertation, Delft University of Technology, Delft, The Netherlands, 2004. [Online]. Available: http://www.are101.org/book/Optimized_Permanent_Magnet_Generator_Topologies_For_Direct-Drive_Wind_Turbines.pdf

[8] D. Svechkarenko, J. Soulard, and C. Sadarangani, "Parametric study of a transverse flux generator at no-load using three-dimensional finite element analysis," in Proc. Int. Conf. on Electrical Machines and Systems, ICEMS2009, Tokyo, Japan, 15-18 November 2009, pp. 1-6.

[9] D. Svechkarenko, J. Soulard, and C. Sadarangani, "Performance evaluation of a novel transverse flux generator with 3D finite element analysis," in Proc. Int. Conf. on Electrical Machines and Systems, ICEMS2009, Tokyo, Japan, 15-18 November 2009, pp. 1-6.

[10] E. Schmidt, "3-D finite element analysis of the cogging torque of a transverse flux machine," IEEE Transaction on Magnetics, vol. 41, No. 5, pp. 1836-1839, May 2005.

[11] S. Salwa, and B. Orlik, "Comparison study of permanent magnet transverse flux motors (PMTFMs) for in-wheel applications," in Proc. International Conference on Power Electronics and Drive Systems, PEDS 2009, Taipei, 2-5 Nov. 2009, pp. 96-101.

[12] J. F. Gieras, "Performance characteristics of a permanent magnet transverse flux generator," in Proc. IEEE International Conference on Electric Machines and Drives, San Antonio, USA, 15 May 2005, pp. 1293-1299.

[13] J. F. Gieras, and M. Wing, Permanent Magnet Motor Technology: Design and Application, 2rd ed., Marcel Dekker Inc., New York, 2002.

[14] MATLAB ver. 7.6.0.324 (R2008a), Software Help. 2008.

[15] M. Gyimesi and D. Ostergaard, "Inductance computation by incremental finite element analysis," IEEE Transaction on Magnetics, vol. 35, No. 3, pp. 1119-1122, May 1999.